ELSEVIER

Journal of Biomechanics 40 (2007) 919–929

JOURNAL OF BIOMECHANICS

www.elsevier.com/locate/jbiomech
www.JBiomech.com

Patient-specific model of brain deformation: Application to medical image registration

Adam Wittek[a], Karol Miller[a,*], Ron Kikinis[b], Simon K. Warfield[b]

[a]*Intelligent Systems for Medicine Laboratory, School of Mechanical Engineering, The University of Western Australia, 35 Stirling Highway, Crawley/Perth, WA 6009, Australia*

[b]*Computational Radiology Laboratory, Brigham and Women's Hospital and Harvard Medical School, 75 Francis Street, Boston, MA 02115, USA*

Accepted 27 February 2006

Abstract

This contribution presents finite element computation of the deformation field within the brain during craniotomy-induced brain shift. The results were used to illustrate the capabilities of non-linear (i.e. accounting for both geometric and material non-linearities) finite element analysis in non-rigid registration of pre- and intra-operative magnetic resonance images of the brain. We used patient-specific hexahedron-dominant finite element mesh, together with realistic material properties for the brain tissue and appropriate contact conditions at boundaries. The model was loaded by the enforced motion of nodes (i.e. through prescribed motion of a boundary) at the brain surface in the craniotomy area. We suggest using explicit time-integration scheme for discretised equations of motion, as the computational times are much shorter and accuracy, for practical purposes, the same as in the case of implicit integration schemes. Application of the computed deformation field to register (i.e. align) the pre-operative images with the intra-operative ones indicated that the model very accurately predicts the displacements of the tumour and the lateral ventricles even for limited information about the brain surface deformation. The prediction accuracy improves when information about deformation of not only exposed (during craniotomy) but also unexposed parts of the brain surface is used when prescribing loading. However, it appears that the accuracy achieved using information only about the deformation of the exposed surface, that can be determined without intra-operative imaging, is acceptable. The presented results show that non-linear biomechanical models can complement medical image processing techniques when conducting non-rigid registration. Important advantage of such models over the previously used linear ones is that they do not require unrealistic assumptions that brain deformations are infinitesimally small and brain stress–strain relationship is linear.

Keywords: Brain; Image registration; Finite element method; Geometric and material non-linearity; Explicit time integration

1. Introduction

Therapeutic technologies that are entering medical practice now, such as e.g. gene therapy, nanotechnology devices, focused radiation, lesion generation and robotic surgery, have extremely localised area of therapeutic effect (Bucholz et al., 2004). Therefore, they have to be applied precisely in relation to the current (i.e. intra-operative) patient's anatomy, directly over specific location of anatomic/functional abnormality. This is one of the key challenges faced by surgery as surgical intervention tends to distort the pre-operative anatomy and often leads to misalignment between the actual position of pathology and its position determined from the pre-operative images. A typical example is a craniotomy (i.e. opening of the skull)—a common neurosurgical procedure that results in the brain shift and tumour movement associated with the shift. Exact physiological mechanisms behind the craniotomy-induced brain shift are hotly disputed among neurosurgical community.

*Corresponding author.
E-mail address: kmiller@mech.uwa.edu.au (K. Miller).

0021-9290/$ - see front matter © 2006 Elsevier Ltd. All rights reserved.
doi:10.1016/j.jbiomech.2006.02.021

While the intra-operative imaging would be the most straightforward method when determining the current position of a tumour and other pathologies during surgery, its quality suffers from the constrains of the operating room. As a result of these constrains, spatial resolution and contrast of intra-operative images are typically inferior to those of pre-operative ones (Warfield et al., 2005). This problem can, in principle, be solved by aligning (i.e. registering) the high-quality pre-operative data to scans of the brain acquired intra-operatively, retaining the pre-operative image quality during the surgery. To achieve accurate alignment, the brain deformation must be taken into account, which implies non-rigid registration. In the past, non-rigid registration relied on purely image-based methods such as optical flow (Beauchemin and Barron, 1995; Dengler and Schmidt, 1988), mutual information-based similarity (Viola and Wells III, 1997), entropy-based alignment (Warfield et al., 2001), and block matching (Dengler and Schmidt, 1988). These methods do not take into account mechanical properties of anatomical structures depicted in the image and may yield non-physical deformation fields. To ensure plausibility of the predicted deformation field, biomechanical models should complement image-based methods. In most practical cases, such models utilise the finite element method (Bathe, 1996) to solve sets of partial differential equations governing the deformation behaviour of continua.

Selection of appropriate mathematical model governing the deformation is crucial to ensure realistic computer simulation of brain deformation. In non-rigid image registration, with one notable exception of Xu and Nowinski (2001), linear solid-mechanics formulation has been used (Ferrant et al. 1999, 2001, 2002; Castellano-Smith et al., 2001; Hagemann et al., 1999; Spicer et al., 2004; Warfield et al., 2000, 2005). In this formulation, brain deformations are regarded as infinitesimal (i.e. geometric linearity) and brain tissue is treated as an elastic material, in which the stress is a linear function of the strain (i.e. material linearity). Although non-rigid registration using linear biomechanical models has been an important achievement that significantly adds to the value of intra-operative imaging (Warfield et al., 2005), it should be realised that neither the assumption about the infinitesimally small brain deformation nor the one about the brain stress–strain linear behaviour is valid during brain shift. Craniotomy typically results in deformation of brain surface as large as 10 mm (Miga et al., 2003) (i.e. around 10% of distance between the left and right cortical landmarks) and rigid-body movement of the brain (Figs. 1 and 2), which implies that non-linear finite element formulations and material models are needed when predicting deformation field within the brain during a typical brain shift.

Therefore, in the previous publication by Wittek et al. (2005) we proposed that when conducting non-rigid registration, medical imaging should be complemented by biomechanical models based on non-linear finite element formulations rather than linear ones. Such models can be integrated using either explicit or implicit methods. In the present study, we demonstrate that non-linear finite element models analysed using explicit rather than implicit integration can facilitate efficient and sufficiently accurate prediction of deformation field within the brain even when simplified brain geometry and limited data about the brain surface deformation are used.

2. Methods

2.1. Construction of finite element mesh for patient-specific brain model

Suitable grids (i.e. finite element mesh in the present study) are required so that computational analysis of geometrical information contained within radiographic images (magnetic resonance images in the present study)

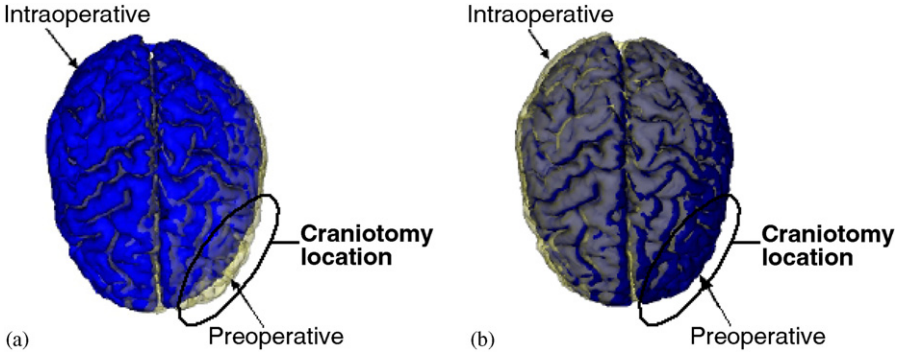

Fig. 1. Comparison of the brain surface determined from images acquired pre-operatively with the one determined intra-operatively from the images acquired after craniotomy. Superior (i.e. "top") view. (a) Pre-operative surface is semi-transparent; (b) Intra-operative surface is semi-transparent. Deformation of brain surface due to craniotomy is clearly visible. Surfaces were determined from the images provided by Department of Surgery, Brigham and Women's Hospital (Harvard Medical School, Boston, Massachusetts, USA).

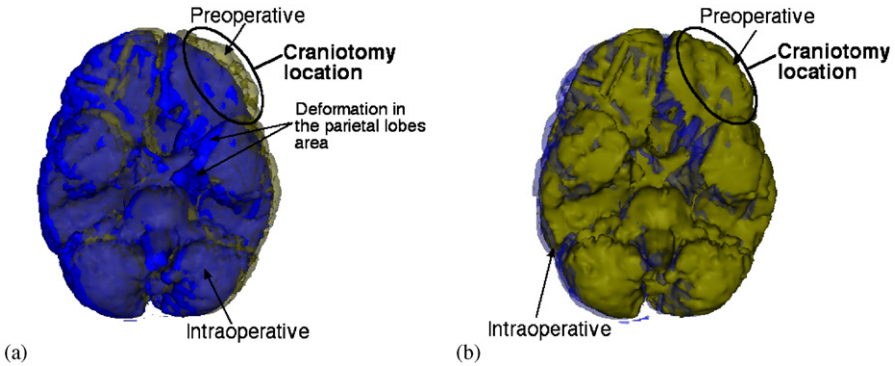

Fig. 2. Comparison of the brain surface determined from images acquired pre-operatively with the one determined intra-operatively from the images acquired after craniotomy. Inferior (i.e. "bottom") view. (a) Pre-operative surface is semi-transparent. Notice lateral deformation of left parietal lobe surface (shift to the right); (b) Intra-operative surface is semi-transparent. Deformation of brain surface due to craniotomy on both craniotomy side and the side opposite to craniotomy is clearly visible. Surfaces were determined from the images provided by Department of Surgery, Brigham and Women's Hospital (Harvard Medical School, Boston, Massachusetts, USA).

can be conducted. Vast majority of studies on surgery simulation rely on tetrahedral meshes (i.e. 4-noded "prisms") as they can be generated automatically even for complex geometries. However, we used hexahedral finite elements (i.e. 8-noded "bricks") with linear shape functions and hourglass control (Belytschko and Bindeman, 1993) as they are a preferable choice when simulating incompressible continua such as the brain. Meshes consisting of such elements perform well for Poisson's ratios close to 0.5. In contrast, those constructed of 4-noded tetrahedrons with linear shape functions tend to lock (i.e. become overly stiff) for incompressible and/or nearly incompressible materials unless special countermeasures are applied (Hughes, 1987).

Patient-specific geometric data for the brain mesh were obtained from a set of 60 pre-operative MRIs of a patient undergoing brain tumour surgery at the Department of Surgery, Brigham and Women's Hospital (Harvard Medical School, Boston, Massachusetts, USA). During this surgical procedure CSF was not removed. In order to distinguish between the brain parenchyma, ventricles and tumour, the images were segmented (Fig. 3) using *3D SLICER* (http://www.slicer.org/), open-source software for visualisation, registration, segmentation and quantification of medical data developed by Artificial Intelligence Laboratory of Massachusetts Institute of Technology and Surgical Planning Laboratory at Brigham and Women's Hospital and Harvard Medical School.

After the segmentation, the digital models of surfaces of the brain parenchyma, lateral ventricles (hereafter referred to as ventricles) and tumour were created in *3D SLICER* using the *Visualisation Toolkit* (*VTK*) binary format (Schroeder et al., 2002). These digital models were processed using *ParaView* (http://www.paraview.org/) to create the ventricle and tumour sagittal sections. After the format conversion, the section contour lines were read into the *HyperMesh* mesh generator (Altair Engineering, Troy, Michigan, USA) (Fig. 4). Then, from the section contour lines, the surface and volumetric patches were created using the *HyperMesh* geometry builder module to represent the entire ventricle and tumour volumes. Automatic *HyperMesh* mesh generator was applied to discretise the patches using hexahedral elements, as described in our previous publication (Wittek et al., 2004). This resulted in a brain mesh consisting of 15,031 hexahedral and 19 pentahedral elements (Fig. 5).

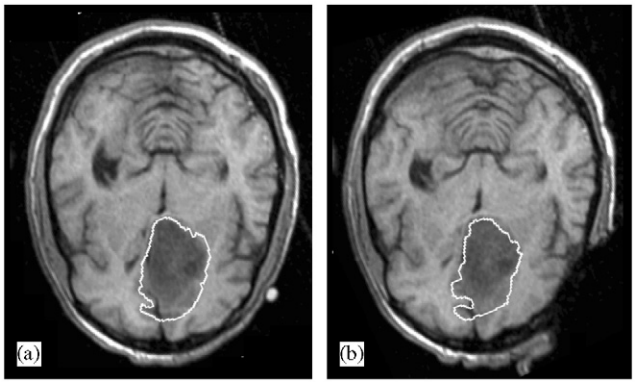

Fig. 3. Segmented MRIs of the head used when building patient specific brain mesh. The tumour segmentation is indicated by white lines in the anterior brain part. (a) Pre-operative; (b) Intra-operative. In this study we used the pre-operative image to build a computational model of the brain, and intra-operative image to measure the displacement of the exposed surface of the brain (used as loading of the model) and to validate computational results. Notice intact tumour in the intra-operative image, i.e. the intra-operative image was taken before tumour excision.

2.2. Computation of brain deformation

2.2.1. Equations of mathematical model

From the perspective of surgical simulation, the brain can be considered a single-phase continuum undergoing

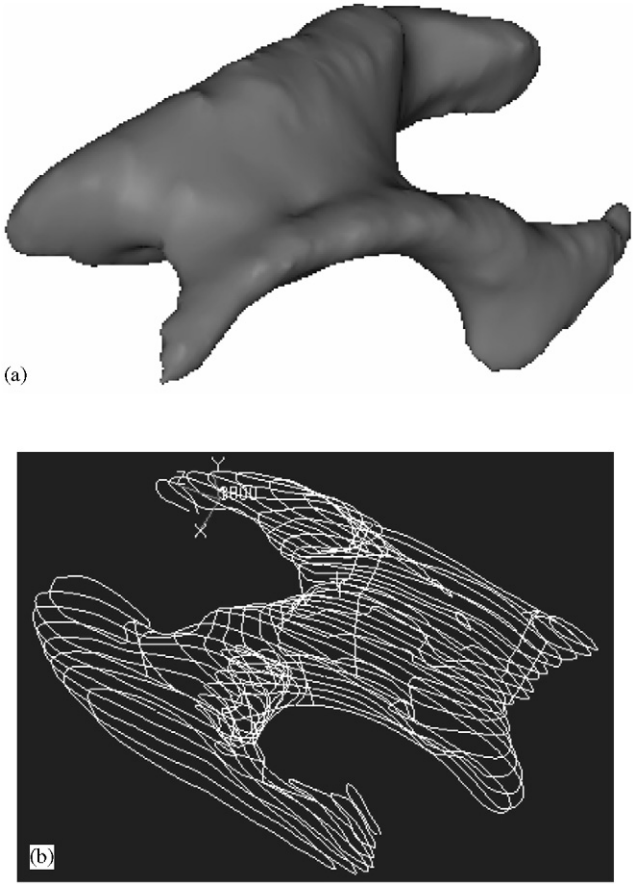

Fig. 4. (a) Ventricle surface model acquired pre-operatively was applied to build the patient specific brain mesh and (b) Ventricle contour lines constructed from this surface model.

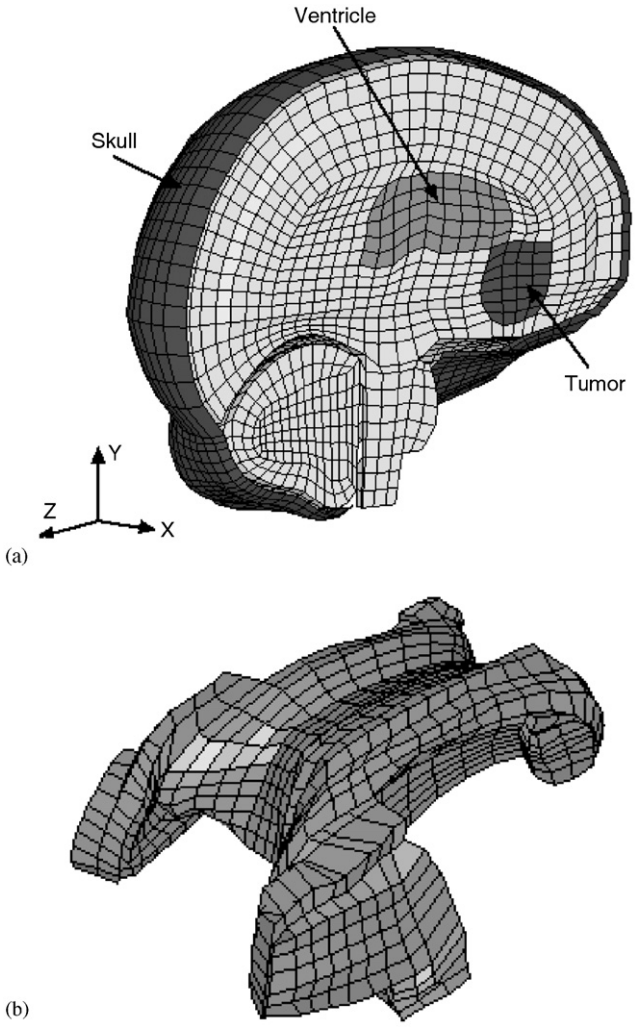

Fig. 5. Patient-specific hexahedron-dominant brain mesh constructed in the present study. (a) Entire left brain hemisphere and (b) lateral ventricles. The element characteristic length varied between 0.6 and 6 mm. For 85% of the elements, the characteristic length was between 2 and 4.5 mm.

large deformations (Miller, 2002). In the present analysis, the stresses and strains were measured with respect to the current configuration. Thus, energetically conjugate Almansi strain ε and Cauchy stress τ (i.e. forces per unit areas in the deformed geometry) were used. Using Almansi strain and Cauchy stress, the virtual work principle, used to derive finite element equations, can be written in the following way:

$$\int_V \tau_{ij}\delta\varepsilon_{ij}\,\mathrm{d}V = \int_V f_i^B \delta u_i\,\mathrm{d}V + \int_S f_i^S \delta u_i\,\mathrm{d}S, \tag{1}$$

where $\int_V \tau_{ij}\delta\varepsilon_{ij}\,\mathrm{d}V$ is the internal virtual work, $\int_V f_i^B \delta u_i\,\mathrm{d}V$ is the virtual work of external body forces, and $\int_S f_i^S \delta u_i\,\mathrm{d}S$ is the virtual work of external surface forces. As the brain undergoes finite deformation, current volume V and surface S, over which the integration is to be conducted, are unknown: they are part of the solution rather than input data. Therefore, appropriate finite element procedures, allowing finite deformation, must be used.

Equations of equilibrium must be supplemented by formulae describing mechanical properties of materials, i.e. appropriate constitutive models. As shown by Miller and Chinzei (1997) and Miller and Chinzei (2002), the stress–strain behaviour of the brain tissue is non-linear. The stiffness in compression is significantly higher than in extension. One can also observe a strong stress–strain rate dependency. To account for these complexities, we used the constitutive model suggested by Miller and Chinzei (2002):

$$W = \frac{2}{\alpha^2}\int_0^t \left[\mu(t-\tau)\frac{\mathrm{d}}{\mathrm{d}\tau}(\lambda_1^\alpha + \lambda_2^\alpha - 3)\right]\mathrm{d}\tau, \tag{2}$$

$$\mu = \mu_0\left[1 - \sum_{k=1}^{n} g_k(1 - \mathrm{e}^{-\frac{t}{\tau_k}})\right], \tag{3}$$

where W is a potential function, λ_i's are principal stretches, μ_0 the instantaneous shear modulus in undeformed state, τ_k's are characteristic times, g_k's are

Table 1
List of material constants for constitutive model of brain tissue, Eqs. (2) and (3), $n = 2$

Instantaneous response	$\mu_0 = 842$ (Pa), $\alpha = -4.7$
$k = 1$	Characteristic time $\tau_1 = 0.5$ (s), $g_1 = 0.450$
$k = 2$	Characteristic time $\tau_2 = 50$ (s), $g_2 = 0.365$

The constants were taken from Miller and Chinzei (2002).

relaxation coefficients, and α is a material coefficient, which can assume any real value without restrictions. The model parameters were taken from Miller and Chinzei (2002) as summarised in Table 1. The constitutive model summarised in Eqs. (2) and (3) belongs to "Ogden-type" class of models. Such models are available in several commercial non-linear finite element codes, e.g. *ABAQUS* (ABAQUS, 1998), *ADINA* (http://www.adina.com), *LS-DYNA* (Hallquist, 1998).

No data on mechanical properties of brain tumour are available in the literature. However, it is commonly acknowledged that tumours and other pathologies are associated with "stiffer" tissue. The volume of the tumour is small as compared to the volume of the brain. Thus, uncertainties about tumour's mechanical properties cannot significantly affect the overall displacement field. Therefore, tumour was simulated using the same constitutive model as "healthy" brain tissue (i.e. hyperviscoelastic material model summarised in Eqs. (2) and (3), and its instantaneous shear modulus was designated a value three times larger than that of brain tissue. Parametric study using values from three times smaller to nine times larger than those for the healthy brain did not show appreciable change in computed displacements.

Ventricles are filled with cerebrospinal fluid (CSF) which has mechanical properties very close to those of water. To mimic this we assigned properties of a very soft compressible elastic solid with Young's modulus E of 10 Pa and Poisson's ratio ν of 0.1 to allow volume decrease during the brain shift.

2.2.2. Loading and boundary conditions

When defining loading for biomechanical models of the brain for image registration one could prescribe forces/pressure due to gravity and interactions between the brain and CSF, e.g. Skrinjar et al. (2001) and Clatz et al. (2003). However, such forces are very difficult to measure/verify and phenomena that produce brain shift are not easily quantified and modelled. Alternative way of defining the loading is to impose displacements on the boundary of continuum (Bathe, 1996), i.e. on the model surface. Brain-image registration can then be described in mathematical terms as follows:

- Known: initial position of the entire domain (as imaged by MRI) and current position of some parts of the boundary, e.g. the displacement of the exposed surface of the brain (as imaged by an intra-operative modality). No surface tractions are applied;
- Unknown: deformation field within the domain (the brain), in particular current position of the tumour.

Problems of this type are very special cases of so called "displacement – traction problems" (Ciarlet, 1988) that have not, to the best of our knowledge, been considered as a separate class and no special methods of solution for these problems exist. Let us call such problems "displacement – zero traction problems". As suggested in papers by Miller (2002, 2005a, 2005b) for such problems the unknown deformation field depends very weakly on the mechanical properties of the continuum. This feature is of great importance in biomechanical modelling where there are always uncertainties in the properties of continuum.

In the present study, brain shift due to craniotomy was considered as a displacement – zero traction problem, and the model was loaded by the enforced motion of nodes (i.e. through prescribed motion of a boundary) at the brain surface in the craniotomy area. The nodal displacements for this motion were determined using intra-operative MRIs although they can be also measured using methods that do not require intra-operative imaging (see e.g. Miga et al., 2003). For both the pre-operatively and intra-operatively acquired cortical surfaces, part of the surface located in the craniotomy area was discretised using rectangular membrane elements, i.e. structured mesh. The same mesh density was used for both surfaces. The distances between corresponding nodes of the discretised pre-operative and intra-operative surfaces were calculated and used as loading (i.e. prescribed nodal displacements).

The formulation of appropriate boundary conditions for computation of brain deformation constitutes a significant problem because of complexity of the brain–skull interface (e.g. see the structure of the tissue layer between the brain and skull in Fig. 1 in Haines et al., 1993). In all the simulations conducted in the present study, rigidity of the skull was assumed while the spine–spinal cord interactions and constraining effects of the spinal cord on the brain rigid body motion were simulated by constraining the spinal end of the model, as summarised in Fig. 6. In order to investigate to what extent the results of brain shift simulation are affected by assumptions made when modelling the brain–skull interface and amount of information about the brain surface deformation when defining the model loading, the brain model summarised in Fig. 5 was analysed using three distinct definitions (referred to as *LBC*1, *LBC*2, and *LBC*3) of the prescribed nodal motion and brain–skull contact.

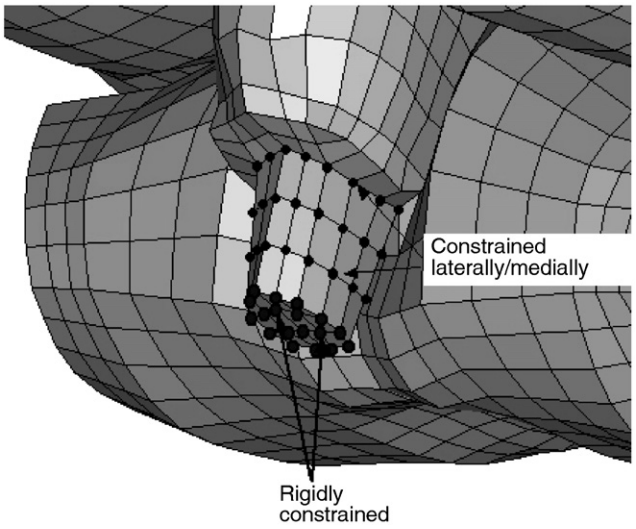

Fig. 6. Boundary conditions at the spinal end of the model. Nodes are indicated by black dots.

*Load case LBC*1*:* No motion of the brain surface relative to the skull was allowed, i.e. there was no gap between the brain and skull in the model. Loading (i.e. enforced displacements) was prescribed only at the nodes located in the exposed (during craniotomy) part of the brain surface as summarised in Fig. 7a. Thus, no intra-operative imaging is necessary to determine the loading and brain–skull boundary conditions for this load case.

*Load case LBC*2: Following Miller et al. (2000, 2005), a gap between the brain and skull was introduced to allow for motion of the brain within the cranial cavity. Introducing of such gap is consistent with an observation that the brain surface located opposite to craniotomy translated laterally by more than 3 mm (Figs. 1 and 2). The brain–skull gap thickness (3.5 mm) was determined from the pre-operative MRIs. As was with case *LBC*1, the loading was prescribed only at the nodes located in the exposed part of brain surface (Fig. 7a), i.e. no information from the intra-operative imaging was required.

*Load case LBC*3: The brain–skull interface was defined in the same way as in load case *LBC*2, i.e. with a brain–skull gap allowing for brain motion within the cranial cavity. Further improvement was done, however, when defining the model loading. The nodal displacements were prescribed not only at the exposed surface but also at the limited number of nodes located in the unexposed area of the brain surface near the craniotomy (Fig. 7b). This requires intra-operative imaging to determine the deformation of the unexposed surface.

For all three definitions of the model loading and boundary conditions, the time histories for enforced motion of boundary nodes were defined using 3-4-5 polynomial (Waldron and Kinzel, 1999) (Fig. 8). This polynomial provides zero velocities and accelerations at

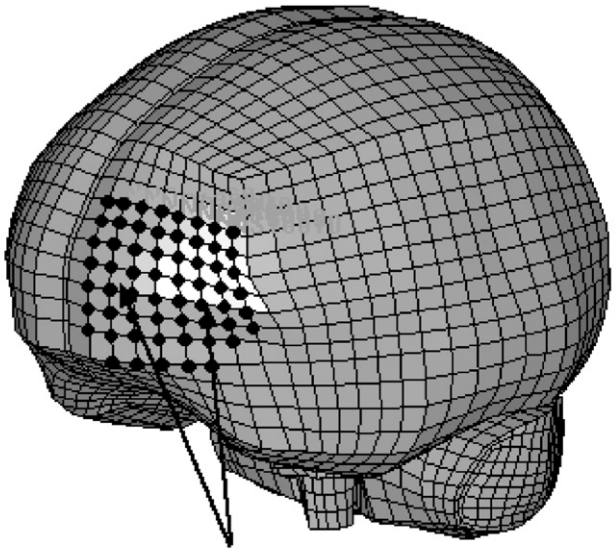

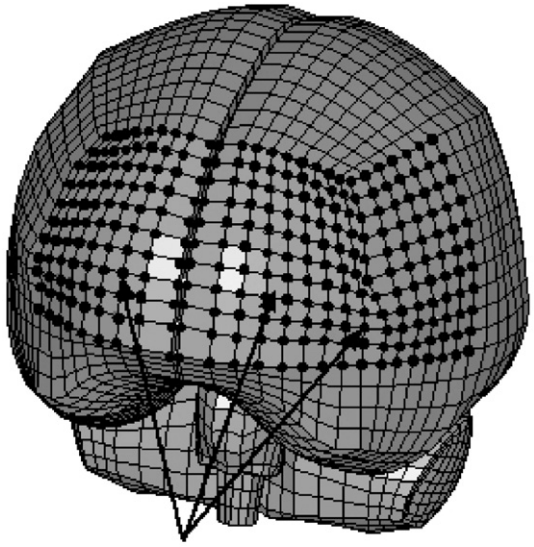

Fig. 7. Model loading through prescribed nodal displacements. (a) Displacements prescribed only at the exposed (during craniotomy) brain surface (loading *LBC*1 and *LBC*2) and (b) Displacements prescribed at exposed and unexposed parts of the brain surface located near the craniotomy (loading *LBC*3).

the beginning and end of loading, which minimises the risk of excitation of loading-induced vibrations.

The present study addresses brain shift induced solely by craniotomy; forced CSF removal and tumour excision were not considered in our analysis.

2.2.3. *Integration of equations of equilibrium*

Integration of equations of equilibrium (or dynamics) in time domain can be done using either implicit or explicit methods (Bathe, 1996; Belytschko, 1976; Crisfield, 1998). The most commonly used implicit integration methods, such as the Newmark's constant

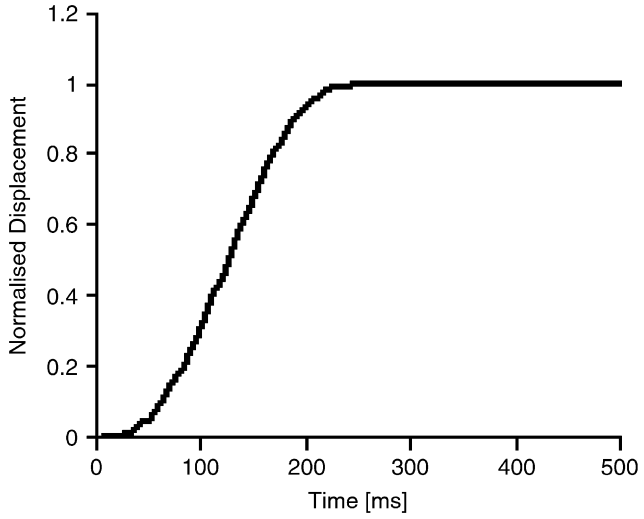

Fig. 8. Normalised time history of loading through enforced motion of boundary nodes. 3-4-5 polynomial (Waldron and Kinzel, 1999) that provides zero velocities and accelerations at the beginning and end of loading was used.

acceleration method, are unconditionally stable. However, they require solution of a set of non-linear algebraic equations at each time step, which involves conducting iterations. Therefore, for large three-dimensional meshes, such as the one used in the present study, the number of numerical operations per each time step can be three orders of magnitude larger than for explicit integration (Belytschko, 1976).

On the other hand, in explicit methods, such as a central-difference method (Belytschko, 1983; Crisfield, 1998), treatment of non-linearities is very straightforward. No iterations are required and computational cost of each time step as well as internal memory requirements are substantially smaller than for implicit integration. These features make explict integration suitable for real-time applications. However, high number of steps may be needed as, normally, severe restrictions on the time-step size have to be included in order to ensure stability of explicit methods. For instance, typical time step in car crash simulations is in the order of magnitude of microsecond (Brewer, 2001; Kirkpatrick et al., 2001). However, as stiffness of brain tissue (Miller, 2002; Miller and Chinzei, 1997, 2002) is eight orders of magnitude lower than that of structural alloys, it is possible to conduct simulations of brain deformation with much longer time steps than in typical dynamic simulations in engineering. For the brain mesh shown in Fig. 5 and material constants as in Table 1, the critical time step is around 2.5×10^{-4} s when the mass density of 1000 kg/m^3 and Poisson's ratio of 0.49 are used. This implies computation with a time step of at least two orders of magnitude longer than that in typical dynamic simulations in engineering.

As explicit integration does not require iterations even for strongly non-linear problems and results in vastly smaller number of numerical operations per time step than implicit integration, it was used as a primary integration method when computing the brain deformation in the present study. The present study appears to be one of the first attempts to apply explicit integration in medical biomechanics when the modelled system undergoes deformation with moderate strain rates.

In order to verify the results obtained using explicit integration, the brain model shown in Fig. 5 was also analysed using implicit integration. We used unconditionally stable Newmark's time integration method (Hughes, 1987) with variable time step (maximum step of 50 ms), and quasi-Newton iterative scheme with Davidon–Fletcher–Powell (DFP) updates (Dennis and More, 1977). The displacement norm was designated a value of 0.001, and the energy norm—a value of 0.01. The global stiffness matrix was inverted using a double precision direct linear-equation solver from BCSLIB-EXT, Boeing's Extreme Mathematical Library (http://www.boeing.com/phantom/bcslib-ext/). Finite element formulation was the same as in explicit integration, i.e. underintegrated hexahedrons with linear shape functions were used.

For both explicit and implicit integrations, the computations were conducted using the *LS-DYNA* (Livermore Software Technology Corporation, Livermore, California, USA) finite element analysis code (Hallquist, 1998).

3. Results

It took around 15 min of computation on personal computer with 2.8 GHz *Pentium* processor to predict brain deformation using explicit time integration. Computed positions of the tumour and ventricles were converted to VTK format (Schroeder et al., 2002) and compared to those measured from the intra-operative magnetic resonance images.

For the loading through enforced motion of boundary nodes located on the exposed brain surface (i.e. directly under the craniotomy) (loading *LBC*1 as in Fig. 7a) and brain–skull contact allowing no brain surface motion, the craniotomy-induced lateral (i.e. in X direction) displacements of the ventricles' and tumour's centres of gravity (COGs) predicted by the model differed by over 2.5 mm from the actual ones determined from the radiographic images (Table 2). The discrepancies were smaller for tumour than for ventricles as the loading (i.e. prescribed nodal motion on the model surface) was applied near the tumour.

Agreement between the computed and observed displacements of the tumour's and ventricles' centres of gravity greatly improved when the gap between the

Table 2
Comparison of craniotomy-induced displacements of tumour and ventricles COGs predicted by the present brain model with the actual ones determined from MRIs

	Determined from MRIs	Predicted			
		Explicit integration			Implicit integration
		Loading *LBC*1	Loading *LBC*2	Loading *LBC*3	Loading *LBC*3
Ventricles	$\Delta x = 3.43$ mm	$\Delta x = 0.90$ mm	$\Delta x = 2.80$ mm	$\Delta x = 3.28$ mm	$\Delta x = 3.38$ mm
	$\Delta y = 0.22$ mm	$\Delta y = 0.25$ mm	$\Delta y = -0.02$ mm	$\Delta y = -0.41$ mm	$\Delta y = -0.28$ mm
	$\Delta z = 1.72$ mm	$\Delta z = 2.45$ mm	$\Delta z = 2.58$ mm	$\Delta z = 2.16$ mm	$\Delta z = 2.17$ mm
Tumour	$\Delta x = 5.34$ mm	$\Delta x = 3.08$ mm	$\Delta x = 4.31$ mm	$\Delta x = 4.76$ mm	$\Delta x = 5.01$ mm
	$\Delta y = -3.45$ mm	$\Delta y = 0.16$ mm	$\Delta y = 0.19$ mm	$\Delta y = -0.49$ mm	$\Delta y = -0.61$ mm
	$\Delta z = 2.60$ mm	$\Delta z = 2.99$ mm	$\Delta z = 2.93$ mm	$\Delta z = 2.73$ mm	$\Delta z = 2.78$ mm

Directions of X, Y and Z axes are given in Fig. 5. Definitions of loading *LBC*1, *LBC*2 and *LBC*3 are given in section *Loading and Boundary Conditions*. Results obtained with tumour shear modulus ranging from three times lower to nine times higher than this of the healthy brain do not appreciably differ and are not shown.

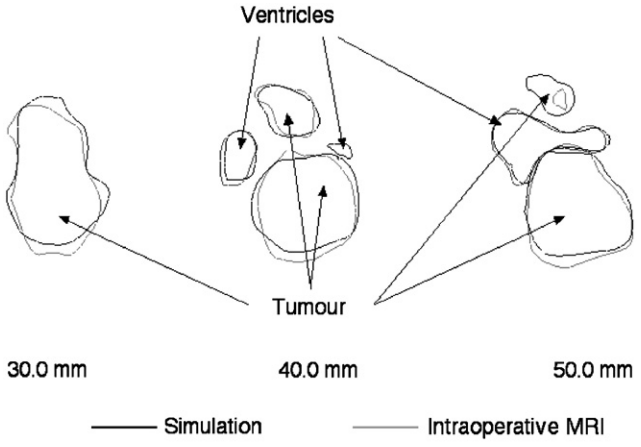

Fig. 9. Load case *LBC*3 (explicit integration). Comparison of contours of coronal sections of ventricles and tumour obtained from the intra-operative images with the ones predicted using the present brain model. Positions of section cuts are measured from the most anterior point of frontal cortex (posterior direction is positive).

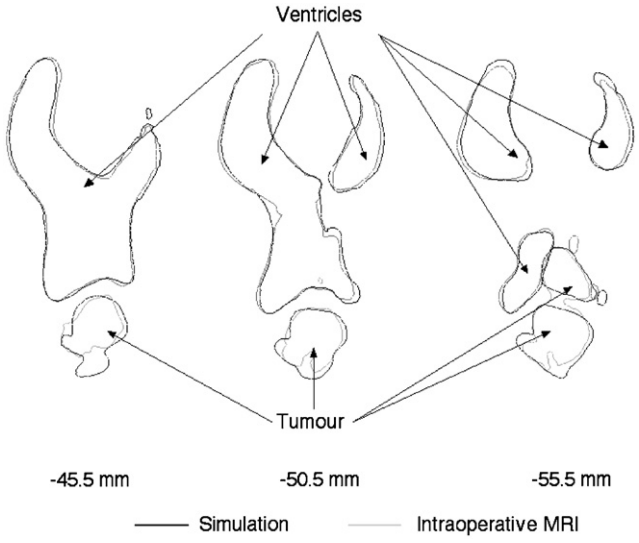

Fig. 10. Load case *LBC*3 (explicit integration). Comparison of contours of axial sections of ventricles and tumour obtained from the intra-operative images with the ones predicted using the present brain model. Positions of section cuts are measured from the most superior point of parietal cortex (superior direction is positive).

brain and skull was introduced (loading *LBC*2). When the loading was also applied to nodes located in the unexposed area of the anterior brain part (loading *LBC*3 as in Fig. 7b), the craniotomy-induced displacements of the ventricles' and tumour's centres of gravity (COGs) predicted by the model agreed well with the actual ones determined from the radiographic images (Table 2). With exception of the tumour COG displacement along the Y (i.e. inferior–superior) axis, the differences between the computed and observed displacements were below 0.60 mm.

Detailed comparison of cross-sections of the actual tumour and ventricle surfaces acquired intra-operatively with the ones predicted by the present brain model indicates some local miss-registration, particularly for tumour (Fig. 9). However, the overall agreement is remarkably good (Figs. 9 and 10). In our opinion, the miss-registration of the tumour visible in 30 mm slice in Fig. 9 is an artefact of image segmentation. The model was created based on segmented pre-operative images. The validation used segmented intra-operative images. As segmentation is a difficult, subjective process, it introduces uncertainty.

Reliability of the results obtained using explicit integration was confirmed by computing the present brain model using Newmark's implicit integration scheme. The displacements of COGs of ventricles and tumour obtained using implicit integration differed by up to only 0.25 mm from those for explicit integration (right most column of Table 2). In contrast, the

computation time for implicit integration (around 3 h 35 min) was order of magnitude longer than for the explicit one (around 15 min).

4. Discussion and conclusions

In the present study, we computed the deformation field within the brain resulting from craniotomy-induced brain shift. We used hexahedron-dominant finite element meshes combined with non-linear (i.e. including both geometric and material non-linearities) finite element formulations. We showed the utility of the method in non-rigid registration of brain magnetic resonance images. Oversimplifying assumptions typically used in surgery simulation, such as those regarding the infinitesimally small brain/organ deformation during surgery, were abandoned. Application of explicit (central difference) time integration made it possible to complete the computation of brain deformation in around 15 min on personal computer with 2.8 GHz *Pentium* processor. It can be expected that this time can be decreased to around 60–120 s when state-of-the-art computation platforms are applied, and even further when the code is optimised for computation speed rather than reliability.

The results obtained using explicit integration were verified by analysing our brain model using implicit integration. The displacements of COGs of ventricles and tumour obtained using implicit integration differed by up to only 0.25 mm from those for explicit integration (Table 2). This virtually negligible difference is likely to be related to the fact that the implicit integration was conducted with much longer time step (up to 50 ms) than the explicit one (0.25 ms), which affected the computed contact forces between the brain and the skull. For soft constraint contact formulation used in our study, contact stiffness increases with time step to ensure contact stability even for long time steps. Long computation time was found to be an important drawback of implicit integration method. For implicit integration, more than 3 h were required to complete the brain shift simulation, which is an order of magnitude longer than for explicit integration.

The presented results indicate that quality of image registration is sensitive to the following two factors: (1) amount and resolution of information about craniotomy-induced deformation of brain surface when defining load (i.e. prescribed nodal motion); and (2) representation of boundary conditions for the biomechanical (finite element) brain models. We used three definitions of loading and brain–skull contact (see Section *Loading and Boundary Conditions*). In the first definition (loading *LBC*1), the nodal displacements were prescribed only at the nodes located in the part of the brain surface exposed during craniotomy (Fig. 7a), and brain–skull contact allowed no brain motion within the cranial cavity. As summarised in Table 2, this contact formulation lead to appreciable discrepancies between the computed and MRI-determined displacements of gravity centres of tumour and ventricles. In the second definition of model loading and boundary conditions (loading *LBC*2), following Miller et al. (2000, 2005), the brain–skull contact included a 3.5 mm gap to allow for displacement of nodes located on the brain surface in direction normal and tangential to the skull. The nodal motion was prescribed only in the exposed area of the brain surface. Thus, in principle, no intra-operative imaging is required for the formulation of this model. Introducing the brain–skull gap resulted in decrease of the differences between the computed and MRI-determined displacements of the tumour and ventricles' gravity centres in lateral and anterior–posterior directions to around 1 mm. Further improvement (differences between the computed and MRI-determined lateral and anterior–posterior displacements of the tumour and ventricles' gravity centres of up to only 0.60 mm) was done by prescribing the nodal displacements not only at the exposed surface but also at the limited number of nodes located in the unexposed area of the anterior brain part (loading *LBC*3, Fig. 7b). Although determining deformation of the unexposed brain surface requires intra-operative imaging, only the brain contour needs to be tracked. Thus, the required amount of intra-operative information is much less than when determining position of pathology during surgery using high resolution intra-operative MRIs. Such information can be obtained using imaging modalities more readily available in operating theatres, such as multi-planar MRIs (Iskandar et al., 2004) or ultrasound (Letteboer et al., 2005; Lindseth et al., 2002).

The presented application of non-linear finite element formulations made it possible to obtain very good agreement between the computed and measured displacements and overall deformation of the tumour and ventricles (Figs. 9 and 10). This agreement was achieved using displacement boundary conditions determined from rather limited intra-operative information about the unexposed brain surface deformation (see description of loading *LBC*3 in subsection *Loading and Boundary Conditions in Methods*). When prescribing the nodal displacements only on the exposed brain surface, the discrepancies between the computed and MRI-determined displacements of tumour and ventricles' mass centres in lateral and anterior–posterior directions were around 1 mm. This should be regarded as a reasonable (perhaps even acceptable) accuracy considering the fact that even surgical robots typically operate through incisions not smaller than a few millimetres.

Nevertheless, some local miss-registrations were also present, particularly in the inferior tumour part (Figs. 9

and 10). The local inaccuracies observed here could be related to differences in segmentation of pre- and intra-operative images: the model was constructed based on segmented pre-operative image, and the computed results were compared to the segmented intra-operative image. As segmentation is a difficult and subjective process, some uncertainties are unavoidable.

Presented modelling approach is applicable to craniotomy-induced brain shift as well as other intra-operative events, for which sufficient intra-operative information is available to deduce model loading through the enforced motion of boundaries. Our methods, however, cannot be applied to events involving topology changes to the brain, such as cutting. Therefore, the methods cannot be used to simulate e.g. tumour excision.

The presented results indicate that finite element analysis using non-linear solid mechanics formulations is a powerful method for computing deformation field within soft organs during surgery. Our experience with explicit time integration scheme clearly indicates a potential for practical, intra-operative application (i.e. computation times of up to 60 s) when using state-of-the-art computation platforms. On the other hand, implicit integration does not exhibit such potential, as the computation times are too long.

For reliable brain image registration, a combined approach using both non-linear, appropriate for large deformations, biomechanical models and well-established methods of medical image processing is needed. State-of-the-art image analysis methods, such as those based on optical flow (Beauchemin and Barron, 1995), mutual information-based similarity (Viola and Wells III, 1997), entropy-based alignment (Warfield et al., 2001), and block matching (Dengler and Schmidt, 1988), work perfectly well when the differences between images to be co-registered is not too large. It can be expected that the non-linear biomechanics-based model supplemented by appropriately chosen image analysis methods would provide a reliable method for brain image registration in the clinical setting.

A number of challenges must be met before computer-integrated surgery systems based on computational biomechanical models can become as widely used as computer-integrated manufacturing systems are now. As we deal with individual patients, methods to produce patient-specific models quickly and reliably must be improved. Substantial progress in automatic meshing methods is required, or alternatively mesh-free methods (Liu, 2003) may provide a solution. Computational efficiency is an important issue, as intra-operative applications, requiring reliable results within approximately 60 s, are most appealing. Progress can be made in non-linear algorithms by identifying parts that can be pre-computed, and parts that do not have to be calculated at every time step. Use of the Total Lagrangian formulation of the finite element method (Bathe, 1996; Lance, 2004), where all field variables are related to the original (known) configuration of the system, and therefore most spatial derivatives can be calculated before the simulation commences, during the pre-processing stage, offers such a possibility. Implementation of algorithms in parallel on networks of processors, and harnessing the computational power of graphics processing units provide a challenge for coming years.

Acknowledgements

The financial support of the Australian Research Council (Grant no. DP0343112) is gratefully acknowledged.

The medical images used in the present study were obtained in the investigation supported by NSF ITR 0426558, a research Grant from the Whitaker Foundation and by NIH Grants R21 MH67054, R01 LM007861, P41 RR13218, P01 CA67165 and U41 RR019703.

The authors gratefully acknowledge collaboration of Toyota Central R&D Labs. (Nagakute, Aichi, Japan) in the development of the brain model.

References

ABAQUS, 1998. ABAQUS Theory Manual. Version 5.8. Hibbitt, Karlsson & Sorensen, Inc.

Bathe, K.-J., 1996. Finite Element Procedures. Prentice-Hall, Englewood Cliffs, NJ.

Beauchemin, S.S., Barron, J.L., 1995. The computation of optical flow. ACM Computing Surveys 27, 433–467.

Belytschko, T., 1976. A survey of numerical methods and computer programs for dynamic structural analysis. Nuclear Engineering and Design 37, 23–34.

Belytschko, T., 1983. Overview of semidiscretization and time integration procedures. In: Belytschko, T., Hughes, T.J.R. (Eds.), Computational Methods for Transient Analysis. North-Holland, Amsterdam, pp. 1–65.

Belytschko, T., Bindeman, L.P., 1993. Assumed strain stabilization of the eight node hexahedral element. Computer Methods in Applied Mechanics and Engineering 105, 225–260.

Brewer, J.C., 2001. Effects of angles and offsets in crash simulations of automobiles with light trucks. In: Proceedings of the 17th Conference on Enhanced Safety of Vehicles, Amsterdam, Netherlands.

Bucholz, R., MacNeil, W., McDurmont, L., 2004. The operating room of the future. Clinical Neurosurgery 51, 228–237.

Castellano-Smith, A.D., Hartkens, T., Schnabel, J., Hose, D.R., Liu, H., Hall, W.A., Truwit, C.L., Hawkens, D.J., Hill, D.L.G., 2001. Constructing patient specific models for correcting intraoperative brain deformation. In: Proceedings of the Fourth International Conference on Medical Image Computing and Computer-Assisted Intervention MICCAI. Lecture Notes in Computer Science, vol. 2208, Utrecht, The Netherlands, pp. 1091–1098.

Ciarlet, P.G., 1988. Mathematical Elasticity. North-Hollad, The Netherlands.

Clatz, O., Delignette, H., Bardinet, E., Dormont, D., Ayache, N., 2003. Patient-specific biomechanical model of the brain: application to Parkinson's disease procedure. In: Proceedings of the International Symposium on Surgery Simulation and Soft Tissue Modeling, IS4TM'03, Juan-les-Pins, France.

Crisfield, M.A., 1998. Non-linear dynamics. In: Non-linear Finite Element Analysis of Solids and Structures. Wiley, Chichester, pp. 447–489.

Dengler, J., Schmidt, M., 1988. The dynamic pyramid—a model for motion analysis with controlled continuity. International Journal of Pattern Recognition and Artificial Intelligence 2, 275–286.

Dennis, J.E., More, J.J., 1977. Quasi-Newton methods, motivation and theory. SIAM Review 19, 46–89.

Ferrant, M., Nabavi, A., Macq, B., Jolesz, F.A., Kikinis, R., Warfield, S.K., 2001. Registration of 3-D intraoperative MR images of the brain using a finite element biomechanical model. IEEE Transactions on Medical Imaging 20, 1384–1397.

Ferrant, M., Nabavi, A., Macq, B., Black, P.M., Jolesz, F.A., Kikinis, R., Warfield, S.K., 2002. Serial registration of interoperative MR images of the brain. Medical Image Analysis 6, 337–359.

Ferrant, M., Warfield, S.K., Guttmann, C.R.G., Mulkern, R.V., Jolesz, F.A., Kikinis, R., 1999. 3D image matching using a finite element based deformation model. In: Proceeding of the Second International Conference on Medical Image Computing and Computer Assisted Intervention MICCAI. Lecture Notes in Computer Science, wl. 1679, Springer, Berlin, pp. 202–209.

Hagemann, A., Rohr, K., Stiehl, H.S., Spetzger, U., Gilsbach, J.M., 1999. Biomechanical modeling of the human head for physically based, nonrigid image registration. IEEE Transactions on Medical Imaging 18, 875–884.

Haines, D.E., Harkey, H.L., Al-Mefty, O., 1993. The "subdural" space: A new look at an outdated concept. Neurosurgery 32, 111–120.

Hallquist, J.O., 1998. LS-DYNA Theoretical Manual. Livermore Software Technology Corporation.

Hughes, T.J.R., 1987. The Finite Element Method: Linear Static and Dynamic Finite Element Analysis. Prentice-Hall, Englewood Cliffs, NJ.

Iskandar, B.J., Sansone, J.M., Medow, J., Rowley, H.A., 2004. The use of quick-brain magnetic resonance imaging in the evaluation of shunt-treated hydrocephalus. Journal of Neurosurgery: Pediatrics 101, 147–151.

Kirkpatrick, S.W., Schroeder, M., Simons, J.W., 2001. Evaluation of passenger rail vehicle crashworthiness. International Journal of Crashworthiness 6, 95–106.

Lance, D., 2004. Efficient Finite Element Algorithm for Computation of Soft Tissue Deformations. B.Sc. Thesis, University of Western Australia, Perth.

Letteboer, M.M.J., Willems, P.W.A., Viergever, M.A., Niessen, W.J., 2005. Brain shift estimation in image-guided neurosurgery using 3-D ultrasound. IEEE Transactions on Biomedical Engineering 52, 268–276.

Lindseth, F., Lango, T., Bang, J., Hernes, T.A.N., 2002. Accuracy evaluation of a 3D ultrasound-based neuronavigation system. Computer Aided Surgery 7, 197–222.

Liu, G.R., 2003. Mesh Free Methods: Moving Beyond the Finite Element Method. CRC Press, Boca Raton.

Miga, M.I., Sinha, T.K., Cash, D.M., Galloway, R.L., Weil, R.J., 2003. Cortical surface registration for image-guided neurosurgery using laser-range scanning. IEEE Transactions on Medical Imaging 22, 973–985.

Miller, K., 2002. Biomechanics of Brain for Computer Integrated Surgery. Publishing House of Warsaw University of Technology, Warsaw.

Miller, K., 2005a. Biomechanics without mechanics: calculating soft tissue deformation without differential equations of equilibrium. In: CD Proceedings of the Sixth Conference on Computer Methods in Biomechanics and Biomedical Engineering, Madrid, Spain, February 2004. FIRST Numerics Ltd., Cardiff, 2005, pp. 8. ISBN: 0-9549670-0-3.

Miller, K., 2005b. Method for testing very soft biological tissues in compression. Journal of Biomechanics 38, 153–158.

Miller, K., Chinzei, K., 1997. Constitutive modelling of brain tissue; experiment and theory. Journal of Biomechanics 30, 1115–1121.

Miller, K., Chinzei, K., 2002. Mechanical properties of brain tissue in tension. Journal of Biomechanics 35, 483–490.

Miller, K., Chinzei, K., Orssengo, G., Bednarz, P., 2000. Mechanical properties of brain tissue in-vivo: experiment and computer simulation. Journal of Biomechanics 33, 1369–1376.

Miller, K., Taylor, Z., Nowinski, W.L., 2005. Towards computing brain deformations for diagnosis, prognosis and neurosurgical simulation. Journal of Mechanics in Medicine and Biology 5 (1), 105–121.

Schroeder, W., Martin, K., Lorensen, B., 2002. Visualization Toolkit: An Object-Oriented Approach to 3D Graphics. Kitware.

Skrinjar, O., Nabavi, A., Duncan, J., 2001. A stereo-guided biomechanical model for volumetric deformation analysis. IEEE Transactions on Biomedical Engineering 20, 95–102.

Spicer, M.A., van Velsen, M., Caffrey, J.P., Apuzzo, M.L.J., 2004. Virtual reality neurosurgery: a simulator blueprint. Neurosurgery 54, 783–798.

Viola, P., Wells III, W.M., 1997. Alignment by maximization of mutual information. International Journal of Computer Vision 24, 137–154.

Waldron, K.J., Kinzel, G.L., 1999. Kinematics, Dynamics, and Design of Machinery. Wiley, New York.

Warfield, S.K., Ferrant, M., Gallez, X., Nabavi, A., Jolesz, F.A., Kikinis, R., 2000. Real-time biomechanical simulation of volumetric brain deformation for image-guided neurosurgery. In: Proceedings of the SC 2000: High Performance Networking and Compting Conference, Dallas, USA.

Warfield, S.K., Rexilius, J., Huppi, P.S., Inder, T.E., Miller, E.G., Wells III, W.M., Zientara, G.P., Jolesz, F.A., Kikinis, R., 2001. A binary entropy measure to assess nonrigid registration algorithms. In: Proceedings of the Fourth International Conference on Medical Image Computing and Computer-Assisted Intervention MICCAI, Utrecht, The Netherlands.

Warfield, S.K., Haker, S.J., Talos, I.-F., Kemper, C.A., Weisenfeld, N., Mewes, U.J., Goldberg-Zimring, D., Zou, K.H., Westin, C.-F., Wells, W.M., Tempany, C.M.C., Golby, A., Black, P.M., Jolesz, F.A., Kikinis, R., 2005. Capturing intraoperative deformations: Research experience at Brigham and Womens's hospital. Medical Image Analysis 9, 145–162.

Wittek, A., Miller, K., Laporte, J., Kikinis, R., Warfield, S.K., 2004. Computing reaction forces on surgical tools for robotic neurosurgery and surgical simulation. In: Proceedings of the Australasian Conference on Robotics and Automation ACRA, Canberra, Australia.

Wittek, A., Kikinis, R., Warfield, S.K., Miller, K., 2005. Brain shift computation using a fully nonlinear biomechanical model. Lecture Notes in Computer Science, vol. 3750, pp. 583–590. Presented at the Eight International Conference on Medical Image Computing and Computer Assisted Surgery MICCAI 2005. Palm Springs, California, USA.

Xu, M., Nowinski, W.L., 2001. Talairach–Tournoux brain atlas registration using a metalforming principle-based finite element method. Medical Image. Analysis 5, 271–279.